Bis-Fe(IV): nature's sniper for long-range oxidation

Jiafeng Geng, Ian Davis, Fange Liu & Aimin Liu

JBIC Journal of Biological Inorganic Chemistry

ISSN 0949-8257
Volume 19
Number 7

J Biol Inorg Chem (2014) 19:1057-1067
DOI 10.1007/s00775-014-1123-8

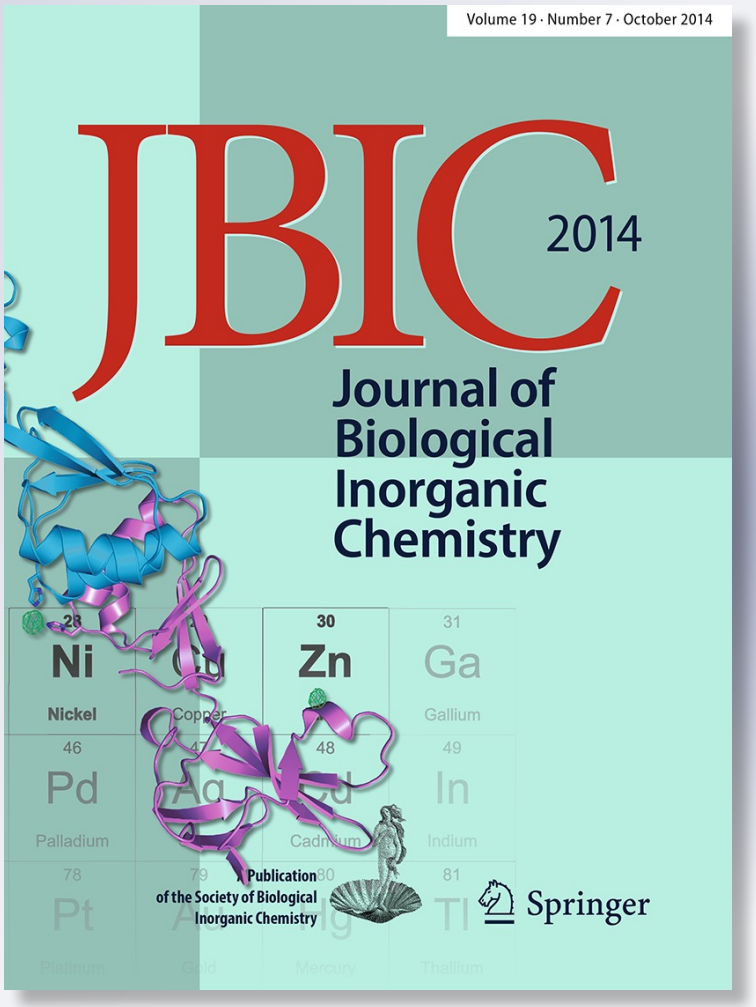

Springer

J Biol Inorg Chem (2014) 19:1057–1067
DOI 10.1007/s00775-014-1123-8

MINIREVIEW

Bis-Fe(IV): nature's sniper for long-range oxidation

Jiafeng Geng · Ian Davis · Fange Liu · Aimin Liu

Received: 6 January 2014 / Accepted: 10 March 2014 / Published online: 11 April 2014

Abstract Iron-dependent enzymes are prevalent in nature and participate in a wide range of biological redox activities. Frequently, high-valence iron intermediates are involved in the catalytic events of iron-dependent enzymes, especially when the activation of peroxide or molecular oxygen is involved. Building on the fundamental framework of iron–oxygen chemistry, these reactive intermediates constantly attract significant attention from the enzymology community. During the past few decades, tremendous efforts from a number of laboratories have been dedicated to the capture and characterization of these intermediates to improve mechanistic understandings. In 2008, an unprecedented bis-Fe(IV) intermediate was reported in a *c*-type diheme enzyme, MauG, which is involved in the maturation of a tryptophan tryptophylquinone cofactor of methylamine dehydrogenase. This intermediate, although chemically equivalent to well-characterized high-valence iron intermediates, such as compound I, compound ES, and intermediate Q in methane monooxygenase, as well as the hypothetical Fe(V) species in Rieske non-heme oxygenases, is orders of magnitude more stable than these other high-valence species in the absence of its primary substrate. It has recently been discovered that the bis-Fe(IV) intermediate exhibits a unique near-IR absorption feature which has been attributed to a novel charge-resonance phenomenon. This review compares the properties of MauG with structurally related enzymes, summarizes the current knowledge of this new high-valence iron intermediate, including its chemical origin and structural basis, explores the formation and consequences of charge resonance, and recounts the long-range catalytic mechanism in which bis-Fe(IV) participates. Biological strategies for storing oxidizing equivalents with iron ions are also discussed.

Keywords High-valent iron · Charge resonance · Long-range catalysis · Radical enzymology · Posttranslational modification

J. Geng · I. Davis · F. Liu · A. Liu (✉)
Department of Chemistry,
Georgia State University,
Atlanta, GA 30303, USA
e-mail: feradical@gsu.edu

Introduction

In recent years, it has come to light that many crucial biological processes are mediated by some of the same culprits which have been implicated in aging and oxidative stress, i.e., activated oxygen species and free radicals. The dual role of these reactive species as both the leading cause of non-specific cell damage and useful catalytic intermediates necessitates that their use in biochemical reactions should be highly specific and strictly controlled. In particular, radical generation and long-range electron transfer (ET) as a means to utilize chemical power is increasingly recognized as an effective strategy for biological systems to perform demanding redox reactions [1–4]. One such example is the biosynthesis of tryptophan tryptophylquinone (TTQ), a protein-derived cofactor that functions as the catalytic center of methylamine dehydrogenase (MADH) [5]. MADH catalyzes the oxidative deamination of methylamine to formaldehyde and ammonia, a process which allows the host bacterium to rely on methylamine to survive [6]. It possesses an $\alpha_2\beta_2$ structure, with each smaller β subunit possessing a TTQ cofactor [7].

TTQ is formed through posttranslational modification of a precursor protein, preMADH. A periplasmic enzyme,

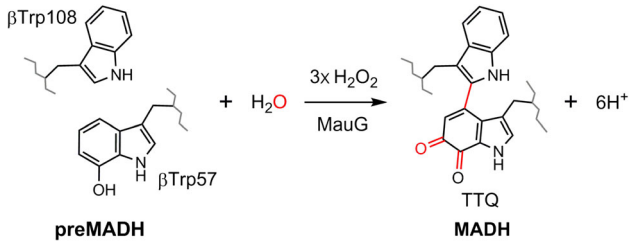

Fig. 1 MauG-catalyzed tryptophan tryptophylquinone (*TTQ*) biosynthesis. Posttranslational modifications of methylamine dehydrogenase (*MADH*) precursor (*preMADH*) are shown in *red*. H_2O_2 serves as a cosubstrate to provide oxidizing equivalents

MauG, uses two *c*-type hemes to mediate this cofactor-maturation process via the oxidation of a tryptophan residue (Trp108) and a monohydroxylated tryptophan residue (Trp57-OH) in the β subunit of preMADH [8, 9]. The latter tryptophan residue is hydroxylated through an uncharacterized mechanism prior to catalytic processing by MauG. The MauG-catalyzed reaction is a three-step, six-electron oxidation process, consisting of cross-link formation between the indole rings of βTrp108 and βTrp57-OH, hydroxylation of cross-linked βTrp108–βTrp57-OH, and quinol-to-quinone oxidation [10] (Fig. 1). Each step requires 1 equiv of H_2O_2 as the oxidant [11]. Alternatively, molecular oxygen can substitute for H_2O_2 as the oxidant in the presence of electron donors such as ascorbate and NADH, yet with a lower catalytic efficiency [11].

Rarely does a hemoenzyme catalyze such a complicated reaction. The involvement of MauG in posttranslational modification of a large protein substrate contradicts our conventional knowledge of the functional behavior of hemoenzymes, which are typically adapted to accommodate their substrates into a heme-binding pocket to facilitate catalysis. Insight into the catalytic strategy used by MauG to perform such unique chemistry began to be revealed by a groundbreaking finding, namely, that the MauG-catalyzed reaction proceeds via an unprecedented high-valence bis-Fe(IV) intermediate [12]. This review is dedicated to discussing our current understanding of this intriguing intermediate and the novel protein radical chemistry that it orchestrates.

MauG, a diheme enzyme involved in protein maturation

The biosynthesis of MADH and its accessory proteins requires a gene cluster named methylamine utilization (*mau*) cluster [13]. The gene that encodes MauG, *mauG*, is located in this cluster. Inactivation of *mauG* in vivo results in the production of an inactive tetrameric $\alpha_2\beta_2$ protein precursor of MADH, preMADH, which contains incompletely synthesized TTQ with monohydroxylated βTrp57 and unmodified βTrp108 [9]. This precursor can be converted to active MADH containing mature TTQ by reaction with H_2O_2 mediated by MauG [11].

In the resting state, MauG binds tightly with its substrate protein, preMADH [14]. It is possible to isolate the MauG–preMADH complex in solution using size-exclusion chromatography [14]. This finding significantly fostered the crystallographic study of MauG; previous efforts to crystallize MauG alone were unsuccessful until co-crystallization of MauG and preMADH was performed. The X-ray crystal structure of the MauG–preMADH complex was subsequently determined [15]. One molecule of preMADH interacts with two molecules of MauG, with each β subunit binding one MauG molecule [15] (Fig. 2a).

MauG possesses two *c*-type hemes in distinct spin states, i.e., a five-coordinate high-spin heme with an axial histidine coordination (denoted as $Heme_{5C}$) and a six-coordinate low-spin heme with an unusual histidine–tyrosine axial ligand set (denoted as $Heme_{6C}$) [8, 15] (Fig. 2b). The two heme iron ions in MauG are separated by 21.1 Å, with the closest edge-to-edge distance between the porphyrin rings being 14.5 Å [15] (Fig. 2b). Despite a large physical separation, the two hemes are able to share electrons efficiently [16, 17]. EPR studies showed that the two hemes are oxidized and reduced in unison rather than sequentially [16]. As such, a clear-cut mixed-valence state cannot be observed. This redox cooperativity suggests that a facile equilibration of electrons occurs between the hemes, allowing them to behave as a single diheme unit rather than as independent redox centers. Notably, owing to its axial coordination vacancy and solvent accessibility, only $Heme_{5C}$ is reactive toward exogenous small molecules [16, 18]. The histidine–tyrosine ligand set at the $Heme_{6C}$ site remains intact regardless of redox events and reactions of MauG [12, 16].

Cytochrome *c* peroxidase–MauG, a functionally diverse diheme superfamily

Structurally, MauG belongs to the cytochrome *c* peroxidase (CcP)–MauG superfamily. This superfamily contains the bacterial diheme CcP (bCcP), MauG, and other diheme peroxidases with unknown functions. Recently, another structurally characterized diheme enzyme, rubber oxygenase (RoxA), has been proposed to be a member of this superfamily [19]. Despite similarities in the overall protein fold, a high degree of functional diversity is present in this superfamily. Different types of reactions are catalyzed by family members sharing a conserved structural core and the same redox cofactors. For instance, bCcP mediates peroxidase reactions in which it transfers the oxidizing equivalents from H_2O_2 to cytochrome *c* or

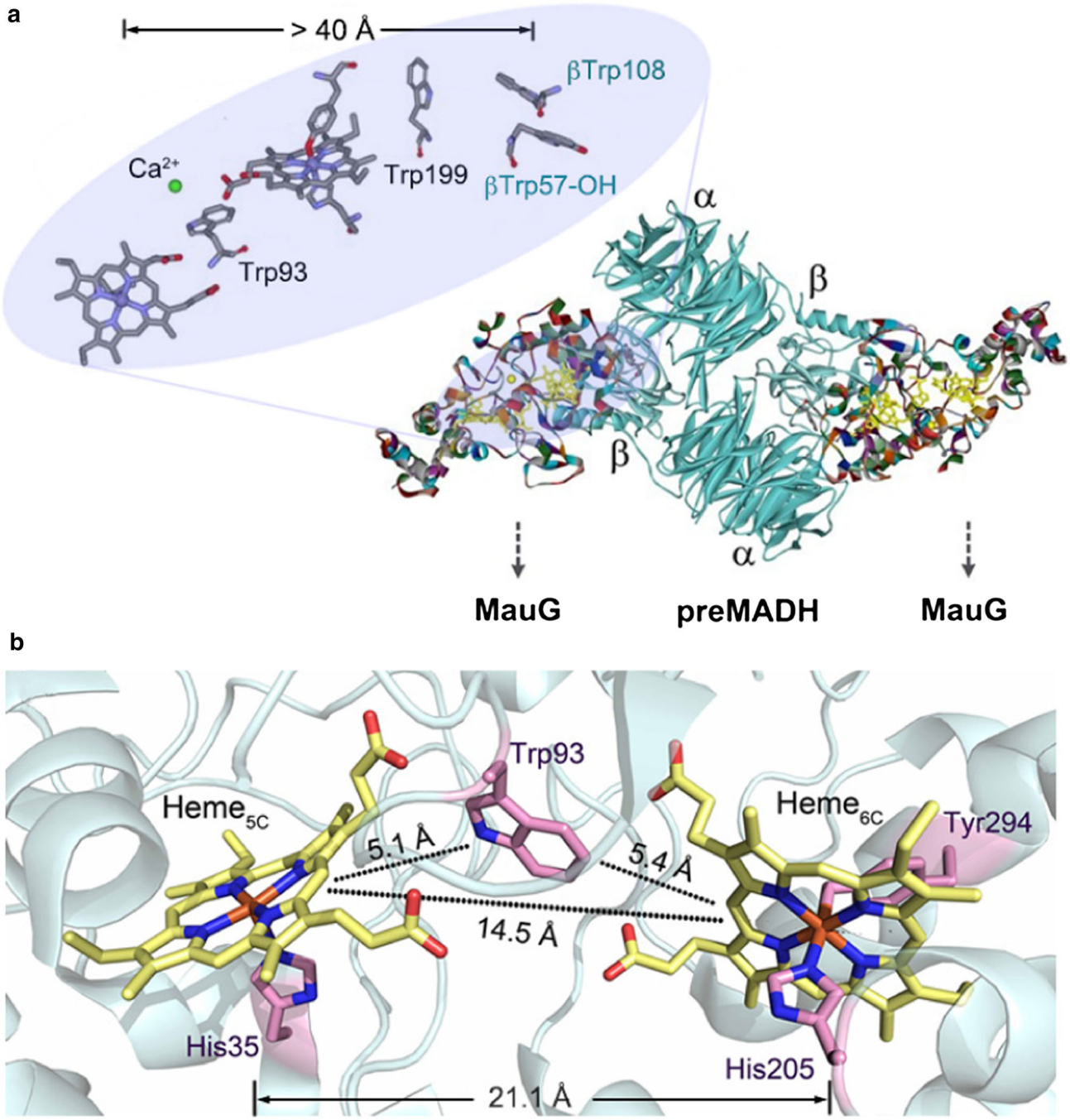

Fig. 2 Crystal structure of MauG [Protein Data Bank (PDB) entry 3L4M]. **a** Overall structure of the MauG–preMADH complex. A zoom-in view of the key redox and structural components along the catalytic pathway is shown in the *left corner*. The center of the two target residues of preMADH are over 40 Å from $Heme_{5C}$ of MauG, the enzyme's "active site" for binding external oxidants. **b** Relative orientation of the hemes and the intervening tryptophan residue. The edge-to-edge distances between the indole side chain of Trp93 and each heme porphyrin ring, and between the two heme porphyrin rings are illustrated. The distance between the two iron centers is also labeled

other small redox proteins, similarly to the functional behavior of monoheme CcPs from other organisms [20]. RoxA, however, catalyzes dioxygenase reactions by incorporating both oxygen atoms of its co-substrate, dioxygen, into latex for rubber biodegradation [19, 21]. Distinct from the former two, MauG orchestrates a complex, multistep redox reaction during TTQ biosynthesis as described above.

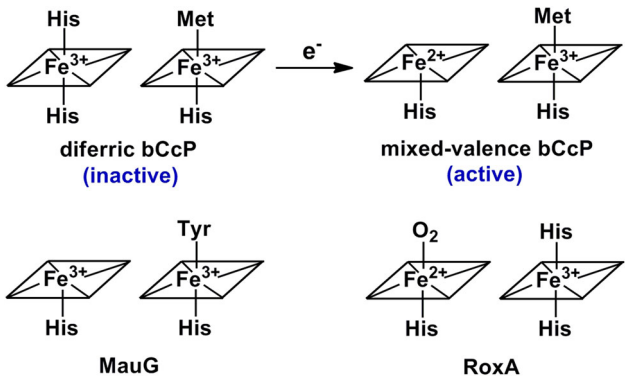

Fig. 3 Axial heme ligand sets in bacterial cytochrome *c* peroxidase (*bCcP*), MauG, and RoxA. The "reductive activation" process in bCcP is illustrated at the *top*; the resting states of MauG and RoxA are presented at the *bottom*. RoxA is isolated with a dioxygen ligand bound to the histidine-coordinated heme [19]

A major determinant of the functional differences between these family members is believed to be the types of axial heme ligands [20, 45]. In the catalytically active form of bCcP, MauG, and RoxA, the reactive heme that binds exogenous oxidant molecules is coordinated by one protein-based ligand, a histidine, whereas the other heme is hexacoordinate with varied axial ligand sets, i.e., histidine–methionine in bCcP [20], histidine–tyrosine in MauG [15], and histidine–histidine in RoxA [19] (Fig. 3). It is noteworthy that the axial ligands of the seemingly less important, hexacoordinate heme play an important role in defining the reaction type and enzymatic functionality by tuning the heme redox properties to control the nature of the reactive intermediates in the catalytic cycle. In bCcP, the thiol ligation to the hexacoordinate heme provided by the conserved methionine residue causes a significantly elevated heme redox potential compared with the other heme. Therefore, mixed-valence states of the diheme cofactor can be generated and are essential to the enzymatic performance in most cases [22, 23]. Despite notable exceptions [24, 25], an Fe(III)/Fe(II) (histidine heme/histidine–methionine heme) mixed-valence state is the common active form of bCcP [20, 26, 27] (Fig. 3). On H_2O_2 binding to the ferric heme, an Fe(IV)/Fe(III) (histidine heme/histidine–methionine heme) mixed-valence state is produced as a result of transfer of the two oxidizing equivalents from H_2O_2 to the diheme cofactor [20, 26, 27]. This mixed-valence intermediate is catalytically competent. During this process, the original ferrous histidine–methionine heme functions as a redox reservoir to safely store one oxidizing equivalent, avoiding the formation of semistable radical species, i.e., compound I and compound ES. In contrast, MauG cannot stabilize a mixed-valence state. The replacement of the methionine ligand with a tyrosine at the hexacoordinate heme site lowers the heme redox potential and facilitates redox cooperativity within the diheme system. As a result, an unprecedented bis-Fe(IV) intermediate, in which both hemes are oxidized to Fe(IV) by H_2O_2, is generated as a key reactive intermediate [12]. The aromatic moiety of the tyrosine ligand also plays an active role in stabilizing the Fe(IV) state via spin delocalization, which counters excess charge built up on the iron center [28].

Although the types of axial heme ligands determine the basic redox chemistry, it is the structural variations outside the conserved folding core that "shape" the substrate specificity of the family members. As shown in Fig. 4, MauG and bCcP share remarkable structural homology [15, 23]. The orientations of several key redox and structural components, including the two *c*-type hemes as well as a conserved tryptophan residue and a Ca^{2+} ion located in between the hemes, are nearly identical. However, notable structural differences are present in four color-coded regions at the protein surface shown in Fig. 4. In MauG, the length of these regions is generally longer than that in bCcP, and three regions are involved in protein–protein interactions with preMADH (Fig. 4a). Most bCcPs are isolated in an inactive diferric state in which one heme has an axial bishistidine ligand set, and the other has a histidine–methionine ligand set [22, 23, 29] (Fig. 3). A "reductive activation" process usually occurs when a one-electron reduction of the high-potential histidine–methionine heme triggers conformational changes both locally and remotely [20, 26, 27]. The conformational changes are localized in 25 % of the molecule [23], and almost overlap with the regions that display structural differences with MauG (Fig. 4b). The remote conformational changes affect the low-potential bishistidine heme site and cause displacement of one of the histidine ligands, allowing H_2O_2 access to that site [22, 23]. The local conformational changes surrounding the histidine–methionine heme may facilitate the binding of small redox proteins to complete the ET process [27]. Therefore, the structural variations on the exterior of the protein are evolutionarily derived to accomplish the substrate specificity of the CcP–MauG superfamily members. This notion is verified by the recent structural characterization of RoxA, which revealed successive accumulation of extensions of peripheral loops [19]. These extended loops may function as "hydrophobic brushes" that can accommodate the entry of the substrate polymer by flexible movements [19].

Bis-Fe(IV) MauG, a lynchpin species in TTQ biogenesis

A striking feature revealed by the crystal structure of the MauG–preMADH complex is that the binding interface between the two proteins is distant from the diheme

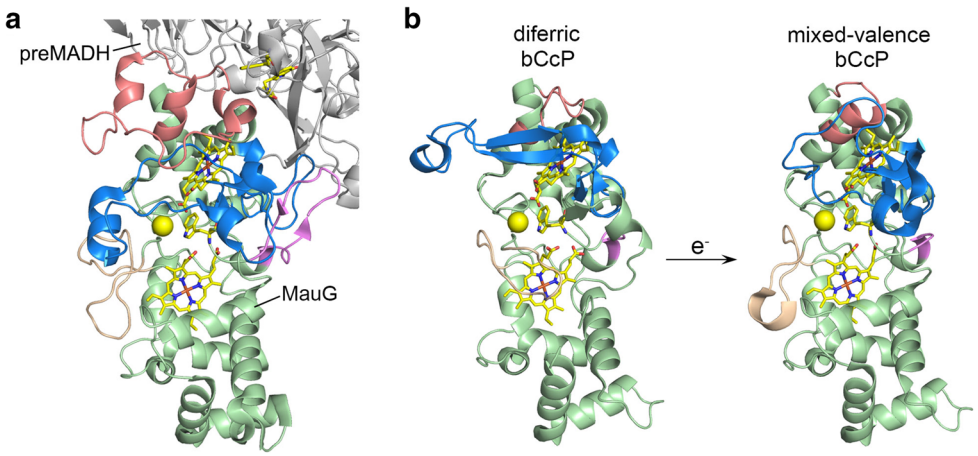

Fig. 4 Structural comparisons between **a** MauG (PDB entry 3L4M) and **b** cytochrome *c* peroxidase (*CcP*) from *Paracoccus pantotrophus* (PDB entries 2C1V and 2C1U). The four regions that show significant structural differences between MauG and bCcP are color-coded. Their corresponding positions are as follows: *red* 292–334 in MauG versus 287–298 in bCcP; *blue* 202–265 in MauG versus 212-260 in bCcP; *violet* 75–90 in MauG versus 102–105 in bCcP; *wheat* 43–63 in MauG versus 77–90 in bCcP. In each structure, the two *c*-type hemes as well as a conserved tryptophan residue and a Ca^{2+} ion located in between the hemes are highlighted in *yellow*. The MauG structure also includes a portion of its binding partner, preMADH, which is shown in *gray*, with the two target tryptophan residues displayed in *yellow*

cofactor [15]. Moreover, the heme that binds H_2O_2, $Heme_{5C}$, is further away from the preTTQ site than $Heme_{6C}$, with a physical distance of over 40 Å [15] (Fig. 2a). Given that the MauG–preMADH co-crystals are catalytically active, a long-range catalytic strategy must be used [30]. Consequently, it has become a legitimate concern as to how the oxidizing power of H_2O_2 is properly delivered to the preTTQ site through the protein matrix of MauG.

The most interesting redox property of MauG is the high-valence state that it stabilizes and uses to catalyze TTQ biosynthesis. On reaction with H_2O_2, a high-valence bis-Fe(IV) species of MauG is generated which spontaneously returns to the resting diferric state on the minute timescale in the absence of preMADH [12] (Fig. 5a). The EPR spectrum of this intermediate showed that both high-spin and low-spin ferric heme signals are not present, suggesting that both hemes are in an EPR-silent Fe(IV) state [12]. Parallel Mössbauer characterization of this intermediate revealed two quadrupole doublets with the following parameters: species 1 with an isomer shift (δ) of 0.06 mm/s and a quadrupole splitting (ΔE_Q) of 1.70 mm/s, and species 2 with $\delta = 0.17$ mm/s and $\Delta E_Q = 2.56$ mm/s [12]. Both isomer shift values are characteristic of Fe(IV) species. Species 1 displays a quadrupole splitting value within the typical range for ferryl and protonated ferryl species [31–35], and is assigned as an Fe(IV)=O species at the $Heme_{5C}$ site (Fig. 5a). Species 2 shows an unusually large quadrupole splitting value which is attributed to an Fe(IV) moiety at the $Heme_{6C}$ site with the original histidine–tyrosine axial ligand set retained (Fig. 5a). The Fe(IV) moiety in bis-Fe(IV) MauG is unique in biology because it lacks an exogenous oxo group which has been observed in all other protein systems and is considered to be crucial for stabilization of the ferryl ion. It is noteworthy that analogous Fe(IV) porphyrin species with two non-oxo axial ligands have been generated in inorganic model complexes and exhibit an uncommonly large quadrupole splitting value as well [36–38]. Together with these observations, the discovery of the bis-Fe(IV) state of MauG suggests that the term "ferryl" should be reserved for Fe(IV) just as "ferrous" and "ferric" are reserved for Fe(II) and Fe(III), respectively, and "oxoferryl" should be reserved for Fe(IV)=O.

Subsequent kinetic characterizations of the bis-Fe(IV) species demonstrated that it is catalytically competent in TTQ biosynthesis [10, 12]. On reaction of the bis-Fe(IV) species with a stoichiometric amount of preMADH, a cationic radical pair of $[\beta Trp57\text{-}OH]^{\cdot+}$ and $[\beta Trp108]^{\cdot+}$ is generated on preMADH as the bis-Fe(IV) species returns to the diferric state [10]. The first step of the MauG-mediated TTQ biosynthesis is then achieved via collision of the radical pair to form a new σ bond between the two tryptophan π moieties. Therefore, the apparent role of the high-valence Fe(IV) ions is to remotely extract electrons from the preTTQ site and generate radical species on it, activating the substrate for reactions. On the basis of this discovery, as well as a crystallographic study which visualized the time-resolved changes at the preTTQ site during catalysis, a mechanistic model for TTQ biosynthesis has been proposed [10]. Specifically, the bis-Fe(IV) species is expected to be involved in each of the two-electron oxidation steps to initiate radical formation on preMADH.

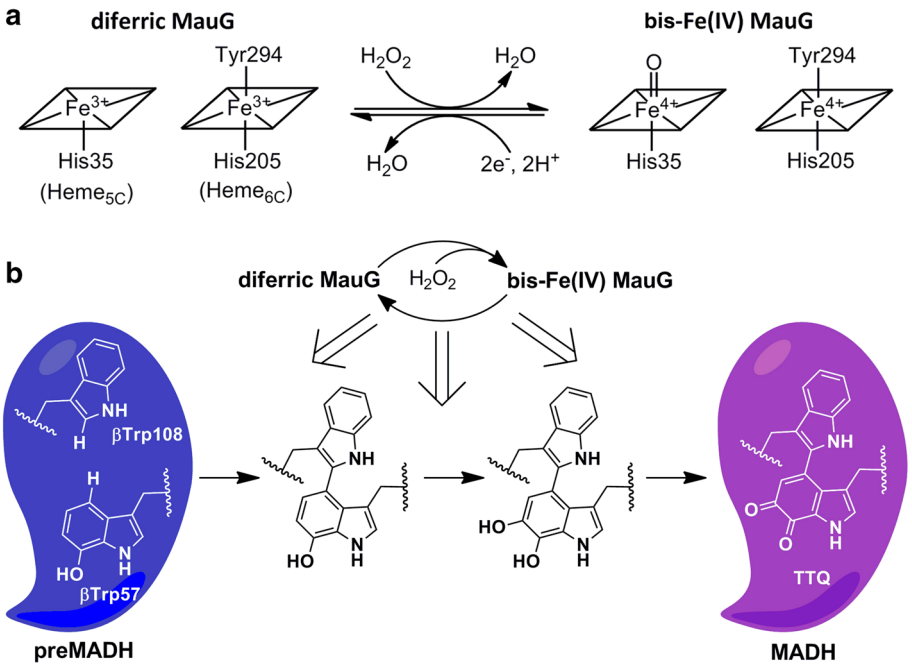

Fig. 5 Bis-Fe(IV) intermediate of MauG. **a** Chemical conversion between diferric and bis-Fe(IV) MauG. **b** Involvement of the bis-Fe(IV) intermediate in TTQ biosynthesis

Radical chemistry occurs at the preTTQ site to accomplish the chemical modifications through sequential reactions of cross-linking, hydroxylation, and oxidation of quinol to quinone (Fig. 5b).

Quite a few protein components spanning the framework of MauG communicate with the diheme cofactor to facilitate the formation and function of the bis-Fe(IV) species. For instance, the axial Tyr294 ligand of Heme$_{6C}$ (Fig. 2b) plays a crucial role in stabilizing the Fe(IV) moiety of Heme$_{6C}$. In its absence, the Fe(IV) state of Heme$_{6C}$ cannot be observed on reaction with H_2O_2 [39, 40]. Consequently, the two oxidizing equivalents derived from H_2O_2 are trapped at the Heme$_{5C}$ site in the form of a compound I-like species [39, 40]. In addition, the Pro107 residue located at the distal pocket of Heme$_{5C}$ is shown to be involved in binding exogenous ligands [41]. This residue also limits the unproductive oxidation of distal methionine residues by bis-Fe(IV) [41, 42]. Trp199 is a surface residue that resides at the protein interface of the MauG–preMADH complex [15] (Fig. 2a). It has been demonstrated that the productive electron flow from the preTTQ site to the bis-Fe(IV) site is achieved through electron/hole hopping with Trp199 as a hopping relay [2]. On mutation of Trp199, the oxidizing power stored at the diheme cofactor can no longer be channeled to the substrate [2]. Moreover, structural studies of MauG revealed the presence of a Ca^{2+} ion in between the two hemes [15] (Fig. 2a). The positioning of the Ca^{2+} ion and the two hemes is essentially identical to that in bCcP (Fig. 4) [22, 23, 29]. In bCcP, the Ca^{2+} ion plays critical structural roles for the enzymatic function. It is required to induce conformational changes around the bishistidine heme during the "reductive activation" process [43]. The presence of the Ca^{2+} ion also governs the dimerization of bCcP, which is active in the dimeric state [44]. The activity of MauG also depends on the presence of the Ca^{2+} ion. Ca^{2+}-depleted MauG is unable to generate the bis-Fe(IV) state [45, 46]. Addition of Ca^{2+} to Ca^{2+}-depleted MauG can restore its reactivity toward H_2O_2 and TTQ biosynthesis activity [45, 46]. EPR and Mössbauer spectroscopic studies have shown that the presence of the Ca^{2+} ion exerts a significant influence on the magnetic properties of the two hemes and the relative orientations of the heme axial ligands: in Ca^{2+}-depleted MauG, Heme$_{6C}$ exhibits a change in the relative orientations of its two axial ligands, and Heme$_{5C}$ is converted to low spin by incorporating another protein residue as its sixth ligand [45]. These changes prevent the enzyme from generating and stabilizing the bis-Fe(IV) state. Given the aforementioned examples, it is evident that an extended network of interactions within the protein matrix is required for MauG to specifically utilize the bis-Fe(IV) species in TTQ biosynthesis.

Charge resonance: a novel mechanism for taming high-valence iron in a biological system

Several intriguing questions have puzzled us since the discovery of the bis-Fe(IV) intermediate in 2008 [12]. Despite being a potent oxidant, the bis-Fe(IV) species displays extraordinary stability in the absence of preMADH, with a half-life of several minutes. What is the

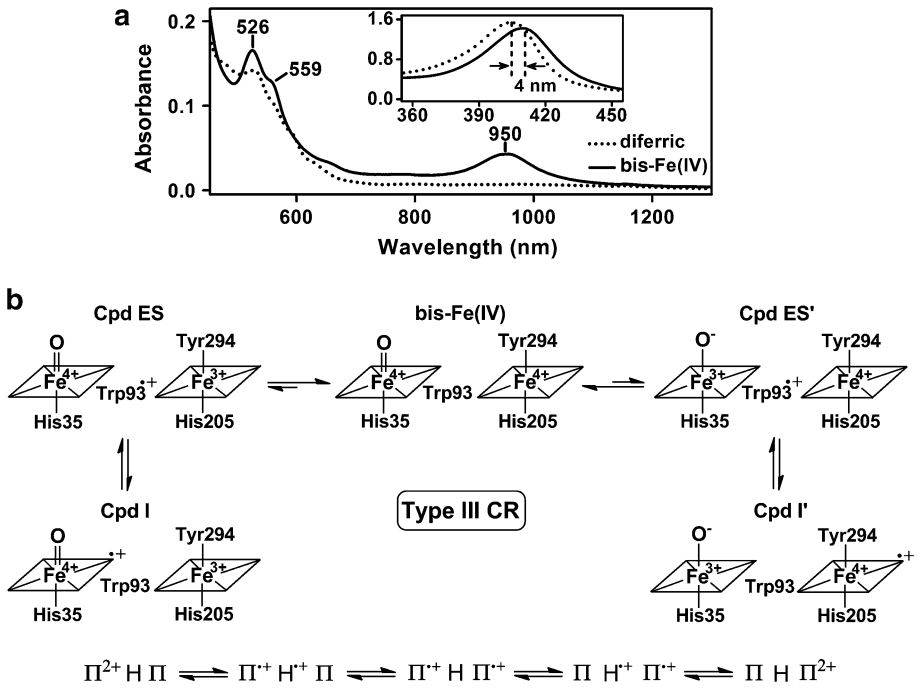

Fig. 6 Tryptophan-mediated charge-resonance (*CR*) transition in bis-Fe(IV) MauG. **a** The bis-Fe(IV) intermediate displays a near-infrared absorption band at 950 nm. The *inset* shows the Soret region of the spectra. **b** Proposed resonance structures for CR transition (type III) in bis-Fe(IV) MauG. *H* represents the hopping site

$$\Pi^{2+}\,H\,\Pi \rightleftharpoons \Pi^{\bullet+}\,H^{\bullet+}\,\Pi \rightleftharpoons \Pi^{\bullet+}\,H\,\Pi^{\bullet+} \rightleftharpoons \Pi\;H^{\bullet+}\;\Pi^{\bullet+} \rightleftharpoons \Pi\;H\;\Pi^{2+}$$

origin of this surprising chemical stability? From another perspective, why does the bis-Fe(IV) species prefer to remotely modify the target tryptophan residues on the substrate protein rather than permanently oxidize its own nearby aromatic residues? The answers to these questions are revealed from a recent finding.

One barrier for understanding the chemical properties of the bis-Fe(IV) species is the lack of a spectroscopic signature for its identification. Recently, a near-infrared (NIR) spectral feature displayed specifically by the bis-Fe(IV) species was discovered [47]. As shown in Fig. 6a, a broad electronic absorption band centered at 950 nm develops on addition of H_2O_2 to diferric MauG. The intensity of this NIR band is maximized at 10 equiv of H_2O_2 [47]. This ratio is consistent with the results of an X-ray absorption spectroscopic study which reported a complete conversion from diferric MauG to bis-Fe(IV) MauG after addition of 10 equiv of H_2O_2 [28]. At this molar ratio of H_2O_2 to MauG, a plot of the intensity of the NIR band against the MauG concentration is linear with a slope of $7.0 \times 10^3\ M^{-1}\ cm^{-1}$ [47]. This value is the molar absorptivity of the NIR band.

It was previously demonstrated that although bis-Fe(IV) MauG is relatively stable, it can be rapidly converted to the diferric state by addition of preMADH [12, 48]. During the decay of bis-Fe(IV) MauG in the absence or presence of preMADH, the time-dependent spectral change of the NIR band occurs concomitantly with time-dependent spectral changes of the heme Soret and Q bands [47]. These observations indicate that the NIR signal arises from bis-Fe(IV) MauG. Further investigations of several MauG mutants with similar or distinct reactivity toward H_2O_2 confirm that the NIR signal is a specific feature of the bis-Fe(IV) state rather than that of a ferryl species in general [47].

The unique NIR band is believed to originate from a charge-resonance (CR) phenomenon [47]. It is known that under certain conditions, an aromatic cation radical can interact with its parent neutral molecule or another molecule of the cation radical to generate noncovalent dimers which exhibit a unique absorption band in the NIR region [49–54]. The NIR spectral feature is a characteristic property of resonance stabilization of the spin and charge within the dimeric complexes and is termed a CR band. There are two classic types of CR transition, i.e., type I CR in a mixed-valence cation radical $\Pi_2^{\cdot+}$ and type II CR in a dication diradical $(\Pi^{\cdot+})_2$ [47]. The former stabilizes an odd number of spin/charge, whereas the latter stabilizes an even number of spin/charge. Notably, ultrafast and reversible ET with a rate constant in the range of 10^7–$10^{11}\ s^{-1}$ is frequently observed between the two monomeric moieties within the CR complexes and is suggested to be essential for delocalization of the spin and charge [55–58]. The spectral characteristics of the NIR band observed in bis-Fe(IV) MauG are highly reminiscent of the CR bands in metalloporphyrin complexes [51, 52]. In MauG, the two oxidizing equivalents derived from H_2O_2 are distributed within the diheme system as two positive charges, giving rise to the bis-Fe(IV) state. This is electronically equivalent to two ferric hemes each coupled with a porphyrin cation radical, a scenario resembling the diradical complexes in type II CR. Hence, the NIR band in bis-Fe(IV) MauG is a putative CR band.

Notably, this case is a unique CR phenomenon because the distance between the two hemes is 14.5 Å (Fig. 2b), much larger than the distances observed in model CR complexes [56, 59]. Trp93, the residue located in between the hemes (Fig. 2), is postulated to be critical for generating this CR phenomenon [47]. The Fe(IV) hemes are sufficiently strong oxidants to oxidize Trp93 as evident from the observation that a minor radical species of Trp93 is always observed along with the bis-Fe(IV) species [12]. Although Trp93 is capable of donating an electron, it cannot fill two holes simultaneously. Since neither the type I nor the type II CR model satisfactorily applies to this case, a new class of CR, type III, is proposed, whereby ET between the high-valence species is facilitated by an additional π system, Trp93 [47] (Fig. 6b). Electron/hole hopping via Trp93 is involved in the ET process between the hemes to make possible CR stabilization of bis-Fe(IV) MauG. Very rapid ET between the hemes with Trp93 as the hopping site mimics the distribution of the spins and charges as if they were in an extended conjugated system.

For the purpose of evaluating the proposed CR model, theoretical calculations have been performed to estimate the ET rate and determine the likely ET mechanism for the ET process between the hemes in bis-Fe(IV) MauG [47]. ET between redox centers can proceed via two different mechanisms, single-step tunneling and multistep hopping. With use of classical ET theory [60], HARLEM calculations [61] were conducted and ET hopping maps [4] were constructed [47]. The ET parameters were calculated for the single-step tunneling pathway between the hemes and the hopping segments between Trp93 and each heme, the latter of which comprise the proposed hopping pathway for the CR transition in bis-Fe(IV) MauG. Both segments exhibit a significantly larger electronic coupling constant (H_{AB}) than the single-step tunneling pathway, suggesting that in the absence of other changes, the ET rate for the hopping mechanism is much larger than that for the single-step tunneling mechanism [47]. Furthermore, hopping maps, which incorporate the influences of thermodynamic factors into the calculation, predict ET rates greater than 10^7 s^{-1} in the bis-Fe(IV) species [47]. This information is in accordance with the reported ET rates for other CR systems. Thus, a hopping mechanism of ET between the hemes mediated by Trp93 explains the observed CR transition in bis-Fe(IV) MauG.

Although it would be more accurate to describe the active oxidant in MauG as an equilibrium between bis-Fe(IV) and other mixed-valence species according to the type III CR model, we continue to use the original description of "bis-Fe(IV)" to avoid potential confusions in the literature. Through CR transition, the oxidizing power of bis-Fe(IV) MauG is harnessed by a trio system of two hemes and a tryptophan residue, endowing this catalytic intermediate with extraordinary stability. This extra layer of control of the chemical power is essential for circumventing uncoupling of the oxidizing equivalents during long-range catalysis. Specifically, the perfect tuning of the redox levels of the related redox components ensures reversible transfer and fast equilibration of electrons/charges among the trio system. This effectively avoids permanent oxidation of the surrounding aromatic residues of bis-Fe(IV), including Trp93, and thus prevents nonproductive leakage of the oxidizing equivalents so that the high-valence iron intermediate never misfires.

Natural strategies for storing two oxidizing equivalents

The discovery and characterization of the bis-Fe(IV) species offers a conceptual contribution to iron–oxygen chemistry and enzymology. Iron-containing enzymes that use oxygen for oxidation and oxygenation reactions usually use high-valence iron intermediates to perform demanding chemical transformations. These intermediates transiently store oxidizing equivalents from peroxide and molecular oxygen and deliver them precisely to the specific substrates to accomplish chemical reactions. During these processes, the iron cofactor plays irreplaceable roles over other transition metals in activating the oxidant molecules and adjusting the chemical reactivity of high-valence intermediates, owing to its ability to access multiple oxidation states. An important topic related to this scientific area is how to store two oxidizing equivalents in ferric iron centers from biological systems. This topic is broadly associated with reactions catalyzed by Rieske non-heme iron-dependent oxygenases, cytochrome P450 oxygenases, and heme-dependent peroxidases.

Notably, a ferric hydroperoxo species is a common intermediate of all three groups of enzymes mentioned above. Release of the two oxidizing equivalents from the hydroperoxo moiety via heterolytic O–O bond cleavage is generally considered as a critical step to initiate productive transformations. Several different strategies have been identified to transiently stabilize the two oxidizing equivalents and channel them to the substrate. Directly storing the two oxidizing equivalents at the ferric iron center results in an Fe(V) species. Thus far, catalytically competent Fe(V) intermediates have only been proposed in Rieske non-heme oxygenases in the form of Fe(V)=O(OH) [62–66] (Fig. 7), but have never been captured in any biological reactions. The severe electron deficiency of the Fe(V) ion makes it extremely destructive to any protein environment as it might oxidize its own coordination ligands or other surrounding residues. Despite the long-standing controversy regarding their involvement in enzymatic reactions, Fe(V) species have been generated in

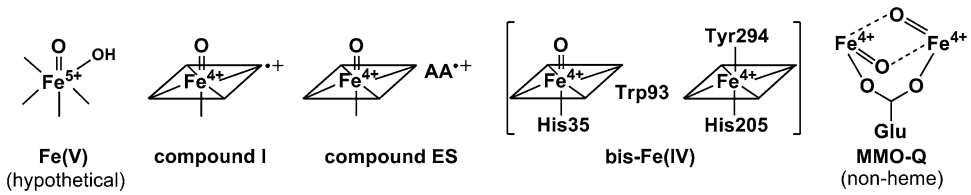

Fig. 7 Electronically equivalent high-valence iron intermediates in biology. *AA* amino acid, *MMO-Q* intermediate Q from methane monooxygenase

synthetic model complexes and have been demonstrated to be capable of performing different reactions, including alkene dihydroxylation reactions [67–69].

In hemoenzymes, it is not practical to have an overly reactive Fe(V) species as a catalytic intermediate, for the heme porphyrin itself is susceptible to oxidation. As a result, an Fe(V) species is generally considered to be a hypothetical intermediate state connecting the starting ferric hydroperoxo species and subsequent reactive high-valence intermediates. The most well-known example of reactive high-valence intermediates in hemoenzymes is the compound I species in P450-type monooxygenases [70–72]. Compound I consists of an oxoferryl ion [Fe(IV)=O] coupled with a π-cation radical located on the heme porphyrin (Fig. 7). It transiently stabilizes two oxidizing equivalents above the ferric state and is chemically equivalent to an Fe(V) species. Delocalization of one oxidizing equivalent over the entire heme moiety, as observed in the compound I species, causes greater chemical stability compared with Fe(V). This modification in reactivity brings great advantages for facilitating enzymatic reactions. During a catalytic cycle, the enzyme active site usually undergoes reorganizations and conformational changes to activate substrates or stabilize transient intermediates. The charge redistribution makes compound I reactive enough to perform the target reaction, yet not so reactive as to cause nonspecific oxidation prior to proper substrate orientation and active-site reorganization.

Another form of high-valence iron species in hemoproteins is compound ES, which is composed of an oxoferryl heme and a nearby aromatic residue-based radical [73] (Fig. 7). Compound ES also contains two oxidizing equivalents above the ferric state. Compared with compound I, the two oxidizing equivalents in compound ES are further separated and the spin-coupling interaction between them is significantly weakened or lost. Therefore, compound ES-type intermediates are frequently used by peroxidases which are capable of performing one-electron oxidation reactions. Moreover, compound ES is reportedly more stable than compound I [74]. The formation of compound ES rather than compound I may be a requirement for enzymes with a larger substrate. For example, in CcP, the reducing equivalents for the compound ES intermediate come from cytochrome *c,* and thus protein–protein interactions are also a part of the catalytic process.

The bis-Fe(IV) species of MauG is the first of its kind and is chemically equivalent to an Fe(V), compound I, or compound ES (Fig. 7). This species has proved a novel natural strategy of storing two oxidizing equivalents in protein-based ferric iron centers. The two oxidizing equivalents of bis-Fe(IV) are stored in two discrete hemes with an intervening tryptophan residue mediating type III CR and exhibit extraordinary stability when the substrate is absent. Notably, the 21-Å separation of the heme irons in the bis-Fe(IV) intermediate distinguishes it from the only other documented protein-based iron intermediate with two Fe(IV) ions, intermediate Q from the non-heme iron-dependent enzyme methane monooxygenase [75] (Fig. 7). Intermediate Q displays an $Fe(IV)_2(\mu\text{-}O)_2$ diamond core structure and is capable of converting methane to methanol [76]. Intermediate Q has a very short Fe–Fe distance (approximately 2.5 Å), and the proximity of the Fe(IV) ions causes them to be strongly coupled [76]. In contrast, the Fe(IV) ions of bis-Fe(IV) MauG are not close enough for direct coupling interactions. In bis-Fe(IV), the delocalization of the oxidizing equivalents over a large area of the protein effectively shifts the chemical power toward the substrate binding site by over 20 Å, making possible the remote electron-abstraction process from the preTTQ site. As mentioned earlier, blocking the charge delocalization by mutating the Tyr294 ligand of $Heme_{6C}$ results in accumulation of a compound I-like species [39, 40]. Although bis-Fe(IV) and compound I may possess similar oxidizing capability, only the former is catalytically competent in TTQ biosynthesis. This comparison highlights the critical role of bis-Fe(IV) in expanding the oxidizing power and shortening the electron-abstraction distance from the substrate.

Bis-Fe(IV) MauG delivers oxidizing power at a distance through a protein radical mechanism

In TTQ biosynthesis, MauG generates a very powerful high-valence iron intermediate, bis-Fe(IV), at one end of the reaction pathway, and uses this potent oxidant to perform "remote enzyme microsurgery" [30] at the other end via protein radical chemistry. At the current stage, it is intriguing to have a "bird's-eye view" of how the oxidizing power initially derived from H_2O_2 is properly delivered to the preTTQ site over 40 Å away through the protein

matrix of MauG. An overview of the reaction pathway of TTQ biosynthesis reveals that the key redox components of ET reactions consist of two types of aromatic moieties, heme and tryptophan (Fig. 2a). The closest distance between the target tryptophan residues at the preTTQ site and the iron center of $Heme_{6C}$ is 19 Å. This gap is bridged by the hopping process through the intervening Trp199 residue [2]. Similarly, the distance between the iron centers of $Heme_{6C}$ and $Heme_{5C}$ is 21 Å, and this gap is spanned by the hopping process through Trp93 [47]. The involvement of these redox components divides the overall ET pathway into small hopping segments, greatly enhancing the ET efficiency. It is noteworthy that the hopping relays (Trp93 and Trp199) are the same kind of residues as the oxidation targets on preMADH. In this case, using the same kind of amino acid for different points in a multistep hopping mechanism is beneficial. The reported ranges of the E_m values for the heme Fe(IV)/Fe(III) and $Trp^{\cdot+}$/Trp redox couples are similar [77, 78], suggesting that the driving force for the reaction of bis-Fe(IV) MauG with preMADH is very low. With use of the same kind of amino acid as staging points, ΔG^0 for each hop will be close to zero. If a different amino acid residue that is more difficult to oxidize is present, the rate of electron hopping from that residue will be lowered. Alternatively, if a residue that is more difficult to reduce is present, the rate of electron hopping into that residue will be lowered.

Although MauG structurally belongs to the CcP–MauG superfamily, from the perspective of the catalytic strategy, it shares more common features with several other enzymes that use radical chemistry to perform long-range chemical reactions, including ribonucleotide reductase [1] and DNA photolyase [79]. In these two enzymes, it is also evident that the overall ET reaction is achieved via electron/hole hopping using the same kind of residues as hopping relays, i.e., tyrosine in ribonucleotide reductase and tryptophan in DNA photolyase. The use of hopping points that are nearly isopotential eliminates effects of ΔG^0 on the ET rates of the hopping steps. It is noteworthy that compared with the other two systems, the overall ET pathway in the MauG–preMADH system has two distinguishable segments: between $Heme_{5C}$ and $Heme_{6C}$, and between $Heme_{6C}$ and preTTQ. In the absence of preMADH, the first segment is able to function independently to stabilize the bis-Fe(IV) species, and the ET process is reversible. This gives rise to the type III CR phenomenon, in which a hopping intermediate, the radical form of Trp93, is observed [47]. In the presence of preMADH, the two segments are connected, and the ET process becomes irreversible as preTTQ, which contains a hydroxylated tryptophan, is easier to oxidize and thus serves as a sink for oxidizing equivalents. In general, the mechanistic study of MauG has supplemented and improved the current knowledge of this emerging group of protein-radical-utilizing enzymes and has generated a profound impact on the broad enzymology community.

Concluding remarks

The MauG–preMADH system is complex, and pursuing an understanding of its chemistry has been full of surprises. It has proved to be a model system to study high-valence iron species, CR phenomena, protein radical chemistry, long-range ET, and protein posttranslational modification. The discovery and characterization of bis-Fe(IV) MauG offers a conceptual contribution to heme chemistry and demonstrates a novel strategy of storing two oxidizing equivalents. This potent intermediate remotely initiates radical formation at the target site of the substrate protein via electron/hole hopping. The substrate itself then directs the sequential transformations of cross-link formation, incorporation of oxygen from the solvent, and quinol-to-quinone oxidation, during the multistep biosynthetic process. Moreover, the type III CR identified in bis-Fe(IV) MauG brings a new concept to this well-documented chemical phenomenon and may serve as a reference to identify similar phenomena in other biological systems.

Acknowledgments The work in the Liu laboratory at Georgia State University on this project has been supported by National Science Foundation grants MCB-0843537 and CHE-1309942, and the Georgia Research Alliance Distinguished Scientist Program (A.L.). We also acknowledge the Molecular Basis of Disease Area of Focus graduate fellowship support to J.G. and the Center for Diagnostics and Therapeutics fellowship support to F.L..

References

1. Minnihan EC, Nocera DG, Stubbe J (2013) Acc Chem Res 46:2524–2535
2. Abu Tarboush N, Jensen LMR, Yukl ET, Geng J, Liu A, Wilmot CM, Davidson VL (2011) Proc Natl Acad Sci USA 108:16956–16961
3. Gray HB, Winkler JR (2010) Biochim Biophys Acta 1797:1563–1572
4. Warren JJ, Ener ME, Vlček A Jr, Winkler JR, Gray HB (2012) Coord Chem Rev 256:2478–2487
5. McIntire WS, Wemmer DE, Chistoserdov A, Lidstrom ME (1991) Science 252:817–824
6. Eady RR, Large PJ (1968) Biochem J 106:245–255
7. Chen L, Doi M, Durley RC, Chistoserdov AY, Lidstrom ME, Davidson VL, Mathews FS (1998) J Mol Biol 276:131–149
8. Wang Y, Graichen ME, Liu A, Pearson AR, Wilmot CM, Davidson VL (2003) Biochemistry 42:7318–7325
9. Pearson AR, De la Mora-Rey T, Graichen ME, Wang Y, Jones LH, Marimanikkupam S, Agger SA, Grimsrud PA, Davidson VL, Wilmot CM (2004) Biochemistry 43:5494–5502
10. Yukl ET, Liu F, Krzystek J, Shin S, Jensen LMR, Davidson VL, Wilmot CM, Liu A (2013) Proc Natl Acad Sci USA 110:4569–4573

11. Li X, Jones LH, Pearson AR, Wilmot CM, Davidson VL (2006) Biochemistry 45:13276–13283
12. Li X, Fu R, Lee S, Krebs C, Davidson VL, Liu A (2008) Proc Natl Acad Sci USA 105:8597–8600
13. Chistoserdov AY, Boyd J, Mathews FS, Lidstrom ME (1992) Biochem Biophys Res Commun 184:1181–1189
14. Li X, Fu R, Liu A, Davidson VL (2008) Biochemistry 47:2908–2912
15. Jensen LMR, Sanishvili R, Davidson VL, Wilmot CM (2010) Science 327:1392–1394
16. Fu R, Liu F, Davidson VL, Liu A (2009) Biochemistry 48:11603–11605
17. Li X, Feng M, Wang Y, Tachikawa H, Davidson VL (2006) Biochemistry 45:821–828
18. Yukl ET, Goblirsch BR, Davidson VL, Wilmot CM (2011) Biochemistry 50:2931–2938
19. Seidel J, Schmitt G, Hoffmann M, Jendrossek D, Einsle O (2013) Proc Natl Acad Sci USA 110:13833–13838
20. Poulos TL (2014) Chem Rev. doi:10.1021/cr400415k
21. Braaz R, Fischer P, Jendrossek D (2004) Appl Environ Microbiol 70:7388–7395
22. Hoffmann M, Seidel J, Einsle O (2009) J Mol Biol 393:951–965
23. Echalier A, Goodhew CF, Pettigrew GW, Fulop V (2006) Structure 14:107–117
24. Arciero DM, Hooper AB (1994) J Biol Chem 269:11878–11886
25. Zahn JA, Arciero DM, Hooper AB, Coats JR, DiSpirito AA (1997) Arch Microbiol 168:362–372
26. Bewley KD, Ellis KE, Firer-Sherwood MA, Elliott SJ (2013) Biochim Biophys Acta 1827:938–948
27. Pettigrew GW, Echalier A, Pauleta SR (2006) J Inorg Biochem 100:551–567
28. Jensen LMR, Meharenna YT, Davidson VL, Poulos TL, Hedman B, Wilmot CM, Sarangi R (2012) J Biol Inorg Chem 17:1241–1255
29. Fülöp V, Ridout CJ, Greenwood C, Hajdu J (1995) Structure 3:1225–1233
30. Bollinger JM Jr, Matthews ML (2010) Science 327:1337–1338
31. Fu R, Gupta R, Geng J, Dornevil K, Wang S, Zhang Y, Hendrich MP, Liu A (2011) J Biol Chem 286:26541–26554
32. Geng J, Dornevil K, Liu A (2012) J Am Chem Soc 134:12209–12218
33. Behan RK, Hoffart LM, Stone KL, Krebs C, Green MT (2006) J Am Chem Soc 128:11471–11474
34. Stone KL, Hoffart LM, Behan RK, Krebs C, Green MT (2006) J Am Chem Soc 128:6147–6153
35. Geng J, Liu A (2014) Arch Biochem Biophys 544:18–26
36. Groves JT, Quinn R, McMurry TJ, Nakamura M, Lang G, Boso B (1985) J Am Chem Soc 107:354–360
37. Bill E, Schünemann V, Trautwein AX, Weiss R, Fischer J, Tabard A, Guilard R (2002) Inorg Chim Acta 339:420–426
38. Ikezaki A, Takahashi M, Nakamura M (2013) Chem Commun 49:3098–3100
39. Abu Tarboush N, Jensen LMR, Feng M, Tachikawa H, Wilmot CM, Davidson VL (2010) Biochemistry 49:9783–9791
40. Abu Tarboush N, Shin S, Geng J, Liu A, Davidson VL (2012) FEBS Lett 586:4339–4343
41. Feng M, Jensen LMR, Yukl ET, Wei X, Liu A, Wilmot CM, Davidson VL (2012) Biochemistry 51:1598–1606
42. Yukl ET, Williamson HR, Higgins L, Davidson VL, Wilmot CM (2013) Biochemistry 52:9447–9455
43. Dias JM, Alves T, Bonifacio C, Pereira AS, Trincao J, Bourgeois D, Moura I, Romao MJ (2004) Structure 12:961–973
44. Prazeres S, Moura JJG, Moura I, Gilmour R, Goodhew CF, Pettigrew GW, Ravi N, Huynh BH (1995) J Biol Chem 270:24264–24269
45. Chen Y, Naik SG, Krzystek J, Shin S, Nelson WH, Xue S, Yang JJ, Davidson VL, Liu A (2012) Biochemistry 51:1586–1597
46. Shin S, Feng M, Chen Y, Jensen LM, Tachikawa H, Wilmot CM, Liu A, Davidson VL (2011) Biochemistry 50:144–150
47. Geng J, Dornevil K, Davidson VL, Liu A (2013) Proc Natl Acad Sci USA 110:9639–9644
48. Lee S, Shin S, Li X, Davidson VL (2009) Biochemistry 48:2442–2447
49. Badger B, Brocklehurst B (1968) Nature 219:263
50. Hausser KH, Murrell JN (1957) J Chem Phys 27:500–504
51. Fajer J, Borg DC, Forman A, Dolphin D, Felton RH (1970) J Am Chem Soc 92:3451–3459
52. Fuhrhop JH, Wasser P, Riesner D, Mauzerall D (1972) J Am Chem Soc 94:7996–8001
53. Lü JM, Rosokha SV, Kochi JK (2003) J Am Chem Soc 125:12161–12171
54. Takai A, Gros CP, Barbe JM, Guilard R, Fukuzumi S (2009) Chem Eur J 15:3110–3122
55. Rosokha SV, Sun D, Kochi JK (2002) J Phys Chem A 106:2283–2292
56. Lindeman SV, Rosokha SV, Sun D, Kochi JK (2002) J Am Chem Soc 124:843–855
57. Sun D, Rosokha SV, Lindeman SV, Kochi JK (2003) J Am Chem Soc 125:15950–15963
58. Heckmann A, Lambert C (2012) Angew Chem Int Ed 51:326–392
59. Song H, Orosz RD, Reed CA, Scheidt WR (1990) Inorg Chem 29:4274–4282
60. Marcus RA, Sutin N (1985) Biochim Biophys Acta 811:265–322
61. Kurnikov IV (2000) HARLEM. Available via http://harlem.chem.cmu.edu/index.php/Main_Page
62. Barry SM, Challis GL (2013) ACS Catal 3:2362–2370
63. Bugg TD, Ramaswamy S (2008) Curr Opin Chem Biol 12:134–140
64. Wackett LP (2002) Enzyme Microb Technol 31:577–587
65. Kovaleva EG, Neibergall MB, Chakrabarty S, Lipscomb JD (2007) Acc Chem Res 40:475–483
66. Chakrabarty S, Austin RN, Deng D, Groves JT, Lipscomb JD (2007) J Am Chem Soc 129:3514–3515
67. Tiago de Oliveira F, Chanda A, Banerjee D, Shan X, Mondal S, Que L Jr, Bominaar EL, Münck E, Collins TJ (2007) Science 315:835–838
68. Prat I, Mathieson JS, Guell M, Ribas X, Luis JM, Cronin L, Costas M (2011) Nat Chem 3:788–793
69. Torres-Alacan J, Das U, Filippou AC, Vohringer P (2013) Angew Chem Int Ed 52:12833–12837
70. Sono M, Roach MP, Coulter ED, Dawson JH (1996) Chem Rev 96:2841–2888
71. Denisov IG, Makris TM, Sligar SG, Schlichting I (2005) Chem Rev 105:2253–2277
72. Rittle J, Green MT (2010) Science 330:933–937
73. Lang G, Spartalian K, Yonetani T (1976) Biochim Biophys Acta 451:250–258
74. Ho PS, Hoffman BM, Kang CH, Margoliash E (1983) J Biol Chem 258:4356–4363
75. Lee SK, Nesheim JC, Lipscomb JD (1993) J Biol Chem 268:21569–21577
76. Shu L, Nesheim JC, Kauffmann K, Münck E, Lipscomb JD, Que L Jr (1997) Science 275:515–518
77. Battistuzzi G, Bellei M, Bortolotti CA, Sola M (2010) Arch Biochem Biophys 500:21–36
78. DeFelippis MR, Murthy CP, Faraggi M, Klapper MH (1989) Biochemistry 28:4847–4853
79. Byrdin M, Villette S, Eker AP, Brettel K (2007) Biochemistry 46:10072–10077